Spectral Characteristics of Asynchronous Data in Operational Modal Analysis

Yi-Chen Zhu[1] and Siu-Kui Au[2]

Institute for Risk and Uncertainty and Centre for Engineering Dynamics

University of Liverpool, United Kingdom

Abstract

Operational Modal Analysis (OMA) has gained popularity for identifying the modal properties of a structure for its high economy and feasibility. Conventionally, time synchronisation among data channels is required to determine mode shape. OMA can be conducted more flexibly if synchronisation is not required. The power spectral density (PSD) matrix of data and its spectral properties are often used for analysing potential modes. Conventionally known properties assume synchronous data and do not carry over to asynchronous data. This paper investigates the spectral properties of asynchronous OMA data. A stationary process with imperfect coherence is proposed that is conducive to OMA while capturing the key asynchronous characteristics. The theoretical properties of PSD matrix are derived and validated using synthetic and experimental data. Although conventional methods do not allow mode shape to be determined from asynchronous data, the present work reveals the possibility by noting that the data are measured under the same excitation and hence share a common PSD in the modal force. Based on this, a simple method is proposed for determining the mode shape. For perfectly incoherent data channels, it is not possible to determine the relative sense of their mode shape values, which is a fundamental limitation of such data. In implementation, the sense can be determined from intuition or estimated from the residual coherence between channels. Experimental application reveals practical issues in OMA with asynchronous data. This work aspires to provide the pathway for more flexible implementation of OMA, e.g., using asynchronous data from multiple smart phones.

[1] Corresponding author. Harrison Hughes Building, Brownlow Hill, Liverpool, L69 3GH, UK. Email: sgyzhu7@liverpool.ac.uk.
[2] Email: siukuiau@liverpool.ac.uk

Key Words: Asynchronous Data, Ambient Modal Identification, Operational Modal Analysis, Spectral Analysis, Vibration Testing

1 Introduction

Modal identification is concerned with extracting the modal properties of a structure based on measured vibration data [1,2]. Modal properties primarily include natural frequencies, damping ratios and mode shapes. They are important quantities demanded in vibration assessment, control or more generally, structural health monitoring [3–5]. Among different classes of modal identification techniques, ambient modal identification, commonly known as 'operational modal analysis' (OMA), has gained popularity in both theory development and practical implementation since it can be conducted under working environmental conditions without artificial loading [6–8]. The input loading is unknown but assumed to be statistically broadband random. Frequency domain decomposition [9] and stochastic subspace identification [10] with its variants are popular conventional techniques in the context of classical ('frequentist') statistics. Other recent techniques include, e.g., blind source identification [11–13], maximum likelihood identification [14,15] and vision-based identification [16]. Bayesian approaches are also available, see review in [17].

To obtain mode shape information, the vibration of a structure at multiple locations, or technically, degrees of freedom (DOF), is measured. Conventional modal identification methods require 'synchronous data', where digital data at different data channels are recorded at the same time scale. In one common experimental configuration, the analogue signals of sensors are transmitted to a central synchronisation hardware (i.e. sampling clock) so that their digitised counterparts are synchronised. NTP (network time protocol) [18] and GPS (global position system) [19] are alternative options to obtain synchronous data. Recently, wireless sensor networks [20–22] are also applied in modal identification tests with several synchronisation schemes [23–25]. Current research mainly discusses synchronisation problems when using wireless sensor networks in modal identification tests, where the time shift between different sensors is a major concern. Asynchronisation problem caused by time shift generally leads to error in both the amplitude and phase of identified mode shapes. This issue was investigated in laboratory and field studies [26–29].

In a more general setting, even when data recording at multiple sensors can be controlled to start and finish at the same time, recording using independent sampling clocks will still

produce asynchronous data. Crystal oscillators (e.g. quartz) are commonly used in data acquisition (DAQ) hardwares to control data sampling process [30]. Although they can provide a frequency reference for sampling time bases with high precision and stability, the actual sampling interval of each oscillator may still vary due to temperature, aging, etc. [31]. The actual sampling intervals between any two clocks are not identical. As long as different data channels are sampled using independent clocks, the measured data will be asynchronous. In this case, conventional analysis techniques that assume synchronous data cannot be directly used. In particular, the singular value (SV) spectrum, i.e., a plot of the eigenvalues of the sample power spectrum density (PSD) matrix, is a conventional tool for visualising the location of potential modes. For synchronous data, in the resonance band of mode(s) the number of lines (eigenvalues) significantly above the remaining ones indicates the number of modes (assuming linealy independent measured mode shapes) and their variation with frequency is similar to the dynamic amplification factor. For a well-separated mode, the eigenvector of the PSD matrix near the natural frequency is a good estimator for the mode shape at measured DOFs. When applied to asynchronous data, however, the SV spectrum exhibits artificial peaks that (when interpreted in the conventional way) incorrectly indicate the presence of multiple extremely close modes with almost identical damping ratios. It is not trivial how modal properties, especially mode shapes, can be correctly determined (if possible) from asynchronous data. On the other hand, there can be significant potential advantages in the economy and convenience of ambient data collection if it is possible to identify modal properties using asynchronous data, although lower identification precision is expected.

Motivated by the above concerns, this paper investigates the theoretical eigenvalue properties of the PSD matrix of asynchronous data in order to explain the characteristics of the SV spectrum and associated eigenvalues calculated from OMA data. The findings are explored to develop a procedure for identifying mode shapes. Asynchronous data is intrinsically a non-stationary process, which is generally more difficult to model or analyse than stationary ones. A stationary process with imperfect coherence is proposed for modelling so that it is conducive to analysis and modal identification, while capturing key asynchronous characteristics within suitable time scales.

The paper is organized as follow. In Section 2, the theoretical eigenvalue properties of the PSD matrix of synchronous OMA data are reviewed. Their characteristics with asynchronous data are introduced and illustrated through an experimental study in Section 3. A stationary stochastic model is proposed in Section 4 for asynchronous OMA data. Based on this model,

the theoretical PSD matrix of data is derived in Section 5. Its eigenvalues and eigenvectors are obtained analytically in terms of modal properties and coherence parameters reflecting the degree of imperfect synchronisation. A simple method is proposed in Section 6 to identify mode shapes from asynchronous data. The proposed theory is validated using synthetic and laboratory experimental data in Section 7. It is also applied to modal identification of a multi-storey structure in Section 8.

2 Power Spectrum and Singular Value Spectrum

The characteristics of eigenvalues and eigenvectors of the PSD matrix of synchronous data near the natural frequency of a mode are first reviewed. They will be compared with their counterparts of asynchronous data in later sections. Time histories of ambient vibration data look erratic as the structure is subjected to different excitation sources (e.g. wind, microtremor, cultural activities) with a variety of frequency characteristics. Working in the frequency domain provides an effective means where activities of different frequency characteristics can be analysed separately. The power spectral density (PSD) spectrum is a plot of the sample PSD of each measured data channel with frequency. Near the natural frequency of a structure, it takes the shape of the dynamic amplification factor of the mode. The singular value (SV) spectrum is a plot of the eigenvalues of the sample PSD matrix with frequency. For synchronous data, the variation of the maximum eigenvalue with frequency takes the shape of the dynamic amplification factor of the mode. The corresponding eigenvector of the PSD matrix near the natural frequency is equal to its partial mode shape confined to the measured DOFs.

Without loss of generality, let the measured acceleration data at n DOFs of a structure be $\{\ddot{\mathbf{x}}_j \in R^n\}_{j=1}^N$, where N is the number of samples per channel. Assuming a classically damped structure with m contributing modes, the data can be modelled as:

$$\ddot{\mathbf{x}}_j = \sum_{i=1}^{m} \boldsymbol{\varphi}_i \ddot{\eta}_i(t_j) + \boldsymbol{\varepsilon}(t_j) \tag{1}$$

where $\boldsymbol{\varphi}_i \in R^n$ is the ith mode shape confined to the measured DOFs; $\ddot{\eta}_i(t_j) \in R$ is the ith modal response of the structure and $\boldsymbol{\varepsilon}(t_j) \in R^n$ is measurement noise. The mode shape is assumed to have unit norm (i.e., $\|\boldsymbol{\varphi}_i\|^2 = \boldsymbol{\varphi}_i^T \boldsymbol{\varphi}_i = 1$). The modal response satisfies the modal equation of motion:

$$\ddot{\eta}_i(t)+2\zeta_i\omega_i\dot{\eta}_i(t)+\omega_i^2\eta_i(t)=p_i(t) \tag{2}$$

where $\omega_i = 2\pi f_i$(rad/s); f_i(Hz) and ζ_i are the natural frequency and damping ratio of the ith mode, respectively; p_i is the ith modal force.

The (scaled) Fast Fourier Transform (FFT) of $\{\ddot{\mathbf{x}}_j\}$ is defined as:

$$\mathcal{F}_k = \sqrt{\frac{2\Delta t}{N}}\sum_{j=1}^{N}\ddot{\mathbf{x}}_j \exp\left[-2\pi\mathbf{i}\frac{(k-1)(j-1)}{N}\right] \tag{3}$$

where $\mathbf{i}^2=-1$ and $\Delta t(\mathrm{s})$ is the sampling interval. Here, $\mathcal{F}_k$ corresponds to frequency $\mathrm{f}_k=(k-1)/N\Delta t$ for $k=1,..,N_q$, where $N_q=\mathrm{int}(N/2)+1$ ($\mathrm{int}(\ )$ denotes the integer part) is the index corresponding to the Nyquist frequency. The FFT is scaled by the factor $\sqrt{2\Delta t/N}$ so that $E[\mathcal{F}_k\mathcal{F}_k^*]$ gives the one-sided PSD matrix, where '*' denotes a conjugate transpose.

Consider a frequency band dominated by a single mode. Within the band, one can model

$$\mathcal{F}_k = \boldsymbol{\varphi}\ddot{\eta}_k + \boldsymbol{\varepsilon}_k \tag{4}$$

where $\boldsymbol{\varphi}$ denotes the mode shape and $\ddot{\eta}_k$ denotes the FFT of modal response; $\boldsymbol{\varepsilon}_k$ is the scaled FFT of measurement noise. The mode index 'i' has been omitted for notational simplicity. Similarly, the natural frequency, damping ratio and the FFT of modal force will be abbreviated as f, ζ and p_k, respectively.

Conventionally, in the resonance band of the mode, modal force is modelled as a stationary stochastic process with a constant PSD; and measurement error as independent and identically distributed (i.i.d.) Gaussian white noise with a constant PSD. For high sampling rate and long duration of data, it is a standard result in time series theory that $\{\mathcal{F}_k\}$ (the collection of FFTs in the band) are asymptotically independent at different frequencies and are jointly 'circularly complex Gaussian' [32]. That is, $\mathrm{Re}\,\mathcal{F}_k$ and $\mathrm{Im}\,\mathcal{F}_k$ are jointly Gaussian vectors and $E[\mathcal{F}_k\mathcal{F}_k^T]=\mathbf{0}$, where ' Re ' and ' Im ' denote the real and imaginary part, respectively.

Post-multiplying $\mathcal{F}_k$ in Eq.(4) by its conjugate transpose and taking expectation gives the theoretical PSD matrix:

$$\mathbf{E}_k = E[\mathcal{F}_k \mathcal{F}_k^*] = SD_k \boldsymbol{\varphi}\boldsymbol{\varphi}^T + S_e \mathbf{I}_n \tag{5}$$

where S is the PSD of modal force; S_e is the PSD of measurement noise; $\mathbf{I}_n$ denotes the $n \times n$ identity matrix and D_k is the dynamic amplification factor:

$$D_k = \left[\left(1-\beta_k^2\right)^2 + \left(2\zeta\beta_k\right)^2\right]^{-1} \qquad \beta_k = f/\mathrm{f}_k \tag{6}$$

The PSD spectrum is a plot of the diagonal elements of $\mathbf{E}_k$ with frequency f_k. A peak in the spectrum indicates the presence of a mode. However, it does not necessarily indicate the number of modes. For example, the PSD spectrum of two data channels measuring the same DOF has two almost identical peaks around the natural frequency of a single mode. The number of modes is reflected in the plot of eigenvalues of $\mathbf{E}_k$, conventionally referred as the 'singular value (SV) spectrum'. The eigenvalues are related to dynamic amplification and eigenvectors to mode shapes. To see this, consider an orthonormal basis $B = \left\{\mathbf{a}_j \in R^n\right\}_{j=1}^n$ with $\mathbf{a}_1 = \boldsymbol{\varphi} \in R^n$ (assuming $\|\boldsymbol{\varphi}\|^2 = 1$). Using this basis, the identity matrix can be written as $\mathbf{I}_n = \sum_{j=1}^n \mathbf{a}_j \mathbf{a}_j^T$. Substituting into Eq.(5) gives the eigenvector representation of $\mathbf{E}_k$:

$$\mathbf{E}_k = \underbrace{\left(SD_k + S_e\right)}_{Eigenvalue} \mathbf{a}_1 \mathbf{a}_1^T + \sum_{j=2}^{n} \underbrace{S_e}_{Eigenvalue} \mathbf{a}_j \mathbf{a}_j^T \tag{7}$$

This indicates that, for a well-separated mode, the largest eigenvalue of the PSD matrix near the natural frequency is equal to $SD_k + S_e$ with eigenvector $\boldsymbol{\varphi}$. The remaining $(n-1)$ eigenvalues are all equal to S_e, reflecting the noise level. In the general case where there can be more than one mode in the band, the number of eigenvalues significantly larger than the remaining ones indicates the dimension of the subspace spanned by the mode shapes, i.e. 'mode shape subspace' [33].

In implementation with a single set of measured data, the PSD and SV spectrum can be estimated by averaging. Given a time history of data $\left\{\ddot{\mathbf{x}}_j\right\}_{j=1}^N$, divide it into M non-overlapping segments, each with $N_w = N/M$ samples. Denote the r th segment by $\left\{\ddot{\mathbf{x}}_j^{(r)}\right\}_{j=1}^{N_w}$, where $\ddot{\mathbf{x}}_j^{(r)} = \ddot{\mathbf{x}}_{N_w(r-1)+j}$. For each segment r, let

$$\hat{\mathbf{E}}_k^{(r)} = \mathcal{F}_k^{(r)} \mathcal{F}_k^{(r)*} \tag{8}$$

where

$$\mathcal{F}_k^{(r)} = \sqrt{\frac{2\Delta t}{N_w}} \sum_{j=1}^{N_w} \ddot{\mathbf{x}}_j^{(r)} \exp\left[-2\pi \mathbf{i} \frac{(k-1)(j-1)}{N_w} \right] \tag{9}$$

The 'averaged PSD matrix' can then be calculated as:

$$\hat{\mathbf{E}}_k = \frac{1}{M} \sum_{r=1}^{M} \hat{\mathbf{E}}_k^{(r)} \tag{10}$$

This is an asymptotically unbiased and consistent estimator for the theoretical PSD matrix. Plotting the diagonal entries and eigenvalues of $\hat{\mathbf{E}}_k$ with frequency gives a smoothed (averaged) version of the PSD and SV spectrum, which are used in practice for visualisation and detection of potential modes. More sophisticated methods are available, e.g., Welch procedure [34].

3 Experimental Illustration of Spectra with Asynchronous Data

The theoretical properties of the PSD matrix derived in the last section assume synchronous data. Their counterparts for asynchronous data have important differences, which shall be illustrated in this section through an experimental study. The experimental evidence forms the basis for the theory to be presented in the next section.

Consider a one-storey laboratory-scale shear building structure as shown in Figure 1. Three piezoelectric accelerometers were placed to measure the acceleration along the weak direction (parallel to paper) under ambient condition (i.e., primarily microtremor at the base). Digital data was sampled at 2048Hz with 24-bit resolution. Within the frequency range of interest (8-12Hz), measurement noise intensity (root PSD) was about $2\times10^{-5}\,\mathrm{g}/\sqrt{\mathrm{Hz}}$ (see the flat line in Figure 3(c) later). Figure 2 shows the experimental setup schematically. Analogue (voltage) signals from Sensor A and B were recorded using the same DAQ device (i.e. the same sampling clock). The signal in sensor C was recorded by another DAQ device (i.e. a different clock). Digital data of the two DAQ devices were sent to the same laptop computer. The two DAQ devices were programmed to acquire ambient acceleration data for two hours with the same start/end time and sampling rate. Clearly, data from Sensor A and B are synchronised. The data from Sensor C is not synchronised with either A or B. In the following discussion, the data from Sensor A and B are combined and referred as the 'synchronous data set'. The data from Sensor A and C are combined and referred as the 'asynchronous data set'.

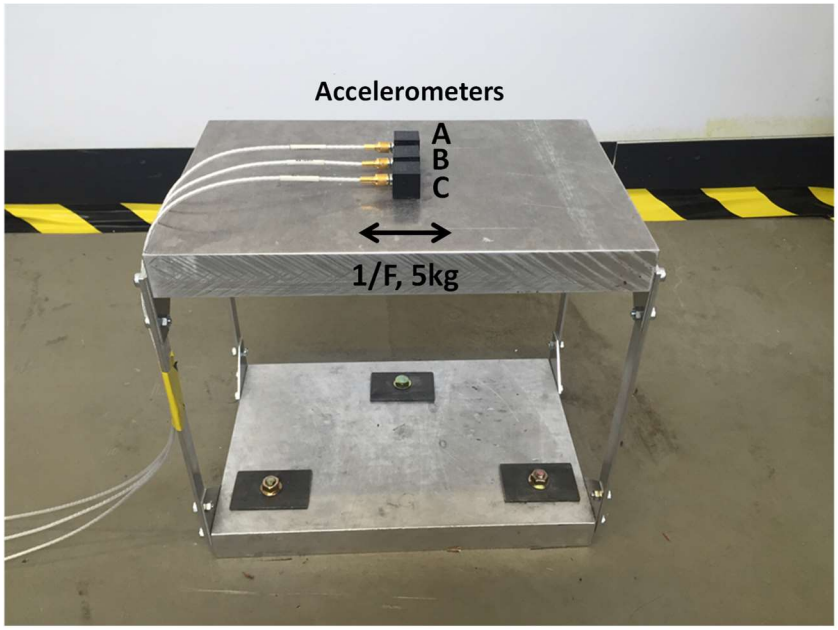

Figure 1. SDOF Shear Frame

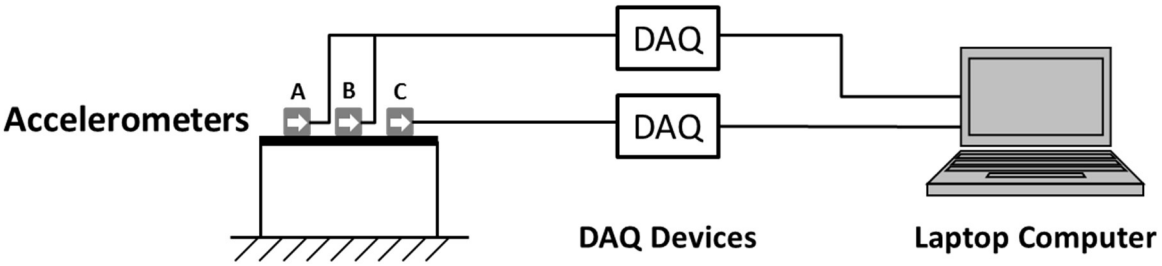

Figure 2. Schematic Diagram of Experiment Setup

The root PSD and SV spectrum for synchronous (left column) and asynchronous (right column) data sets are plotted in Figure 3. The square root of the PSD and SV is plotted as it has a unit $\mathrm{g}/\sqrt{\mathrm{Hz}}$ scaling linearly with g, which is convenient for order of magnitude check. The PSD spectra ((a) and (b)) indicate the presence of a mode around 10Hz. They are almost identical (theoretically they are, see next section) and do not reveal asynchronous nature of data. The latter is revealed in the SV spectra in the second row. According to Eq.(7), there is only one peak when all data channels are synchronised. This is consistent with Figure 3(c). The other line which is almost flat reflects the channel noise level, ranging between $2\times10^{-5}\,\mathrm{g}/\sqrt{\mathrm{Hz}}$ to $3\times10^{-5}\,\mathrm{g}/\sqrt{\mathrm{Hz}}$. However, for the asynchronous data set in Figure 3(d), there are two peaks at almost the same frequency and with almost the same spread (indicative of damping). If one (erroneously) assumes that the data is synchronised (as is typical), the

two peaks will be mistaken as two extremely close modes with similar natural frequency and damping ratio.

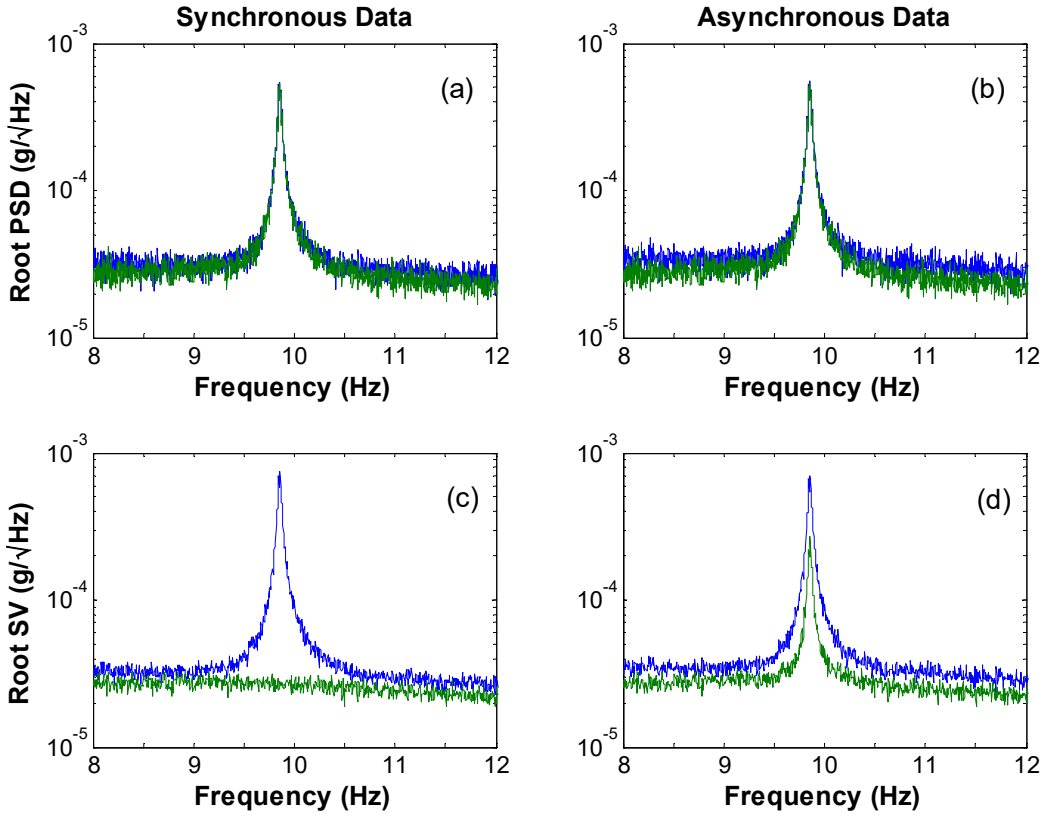

Figure 3. Root PSD and SV Spectrum of Synchronous Data Set (Sensor A & B, Left Column) and Asynchronous Data Set (Sensor A & C, Right Column)

4 Modelling Asynchronous Data

Motivated by the experimental findings in the last section, a model is proposed in this section for asynchronous OMA data. The theoretical properties of its PSD matrix shall be investigated in the next section. The actual sampling time of a DAQ unit consists of the nominal time interval and the random time variation due to 'clock jitter' (resulting from the noise of individual time-measuring oscillators). The sampling time errors caused by clock jitter are accumulated over time. This time-varying behaviour in the sampling instant leads to the non-stationarity of the sampled asynchronous data [35,36]. Non-stationary data is generally much more difficult to model or analyse than stationary ones. A stationary process model is proposed to facilitate analysis and modal identification while capturing key asynchronous characteristics within suitable time scales. The data at different channels are

assumed to start at the same time. This has taken into account of the fact that in reality any initial time shift between channels will be first detected and compensated. After adjustment the effect is negligible compared to the random time drift of different clocks, which is the primary issue in applications with asynchronous data and is the focus of this work.

To see how asynchronous data can be modelled, recall Eq.(4) that applies for synchronous data. For asynchronous data, the same characteristics can be assumed for the measurement noise ($\boldsymbol{\varepsilon}_k$) at different data channels because they are independent regardless of synchronisation. The difference lies in the first term, i.e., the modal contribution. For synchronous data, the modal contributions at different DOFs follow exactly the same time variation according to the same modal response $\ddot{\eta}(t)$, whose FFT is $\ddot{\eta}_k$. This will not be true when different channels are not synchronised.

For discussion purpose, define a 'synchronous data group' as a set of data channels recorded on the same sampling clock. Let the whole measurement array comprise n_g groups. For a given mode shape $\boldsymbol{\varphi}$, let $\mathbf{u}_i \in R^{n_i}$ $\left(i = 1,...,n_g\right)$ denote the part of $\boldsymbol{\varphi}$ measured by Group i and $\ddot{\eta}_{ki}$ be the FFT of the associated modal acceleration responses, where n_i is the number of measured DOFs in Group i. If the groups were all synchronised among each other then $\{\ddot{\eta}_{ki}\}_{i=1}^{n_g}$ would have been identical. The FFT of data in Eq.(4) now reads, for asynchronous data,

$$\mathcal{F}_k = \begin{bmatrix} \mathbf{u}_1 \ddot{\eta}_{k1} \\ \vdots \\ \mathbf{u}_{n_g} \ddot{\eta}_{kn_g} \end{bmatrix} + \boldsymbol{\varepsilon}_k \tag{11}$$

Assume that all data channels are controlled to start recording at the same time with the same number of samples. Otherwise, they can be aligned using existing time delay estimation techniques [37,38]. Each synchronous data group uses its own clock for sampling. Modal contributions in different groups are asynchronised realisations of the same modal response. It is therefore reasonable to assume that $\{\ddot{\eta}_{ki}\}_{i=1}^{n_g}$ are identically distributed. Then

$$E\left(\ddot{\eta}_{ki}\ddot{\eta}_{ki}^{*}\right)=SD_k \qquad i=1,...,n_g \tag{12}$$

Modelling the relationship among the $\left\{\ddot{\eta}_{ki}\right\}_{i=1}^{n_g}$ in a fundamental manner is very challenging because in the first place asynchronous data is a non-stationary process, which is more difficult to model or analyse than stationary ones. To balance model simplicity and utility, a stationary stochastic model is proposed, where asynchronous effect is modelled empirically through imperfect coherence between groups:

$$\chi_{kij}=\frac{E\left(\ddot{\eta}_{ki}\ddot{\eta}_{kj}^{*}\right)}{\sqrt{E\left(\ddot{\eta}_{ki}\ddot{\eta}_{ki}^{*}\right)E\left(\ddot{\eta}_{kj}\ddot{\eta}_{kj}^{*}\right)}} \tag{13}$$

where $\chi_{kij}\in C$ ($\left|\chi_{kij}\right|\le 1$) is the coherence between ith and jth group at frequency f_k. This model is justified for frequencies that are small compared to the reciprocal of the random time difference (drift) between the sampling clocks of different groups.

Using Eq.(11), the PSD matrix for asynchronous data is given by:

$$\mathbf{E}_k=E\left(\mathcal{F}_k\mathcal{F}_k^{*}\right)=SD_k\begin{bmatrix}\mathbf{u}_1\mathbf{u}_1^T & \chi_{k12}\mathbf{u}_1\mathbf{u}_2^T & \cdots & \chi_{k1n_g}\mathbf{u}_1\mathbf{u}_{n_g}^T\\ \chi_{k21}\mathbf{u}_2\mathbf{u}_1^T & \mathbf{u}_2\mathbf{u}_2^T & & \vdots\\ \vdots & & \ddots & \vdots\\ \chi_{kn_g1}\mathbf{u}_{n_g}\mathbf{u}_1^T & \cdots & \cdots & \mathbf{u}_{n_g}\mathbf{u}_{n_g}^T\end{bmatrix}+S_e\mathbf{I}_n \tag{14}$$

The diagonal elements of the PSD matrix $\mathbf{E}_k$ (i.e. the PSD spectrum) for asynchronous data are the same as their synchronous counterparts (see Eq.(5)), which do not reveal the asynchronous nature of data. The latter is reflected in the off-diagonal partitions through the coherence parameters $\left\{\chi_{kij}\right\}$. This changes the eigenvalue properties of $\mathbf{E}_k$, which shall be analysed in the next section.

5 Eigenvalue Properties of PSD Matrix

In this section, the eigenvalues and eigenvectors of the PSD matrix of asynchronous data, i.e., $\mathbf{E}_k$ in Eq.(14), are obtained analytically. It shall be seen that they are determined by the following positive semi-definite matrix $\mathbf{C}_k\in C^{n_g\times n_g}$, which can be seen as a condensed form of the bracketed matrix in Eq.(14):

$$\mathbf{C}_k = diag\left\{\left\|\mathbf{u}_i\right\|\right\}_{i=1}^{n_g} \boldsymbol{\chi}_k diag\left\{\left\|\mathbf{u}_i\right\|\right\}_{i=1}^{n_g}$$
$$= \begin{bmatrix} \left\|\mathbf{u}_1\right\|\left\|\mathbf{u}_1\right\| & \chi_{k12}\left\|\mathbf{u}_1\right\|\left\|\mathbf{u}_2\right\| & \cdots & \chi_{k1n_g}\left\|\mathbf{u}_1\right\|\left\|\mathbf{u}_{n_g}\right\| \\ \chi_{k21}\left\|\mathbf{u}_2\right\|\left\|\mathbf{u}_1\right\| & \left\|\mathbf{u}_2\right\|\left\|\mathbf{u}_2\right\| & & \vdots \\ \vdots & & \ddots & \vdots \\ \chi_{kn_g1}\left\|\mathbf{u}_{n_g}\right\|\left\|\mathbf{u}_1\right\| & \cdots & \cdots & \left\|\mathbf{u}_{n_g}\right\|\left\|\mathbf{u}_{n_g}\right\| \end{bmatrix} \tag{15}$$

where $diag\left\{\left\|\mathbf{u}_i\right\|\right\}_{i=1}^{n_g}$ denotes a diagonal matrix with entries $\left\{\left\|\mathbf{u}_i\right\|\right\}_{i=1}^{n_g}$ and $\boldsymbol{\chi}_k$ denotes a $n_g \times n_g$ matrix with (i,j) entry χ_{kij}. Let $\left\{\lambda_{ki} \geq 0\right\}_{i=1}^{n_g}$ and $\left\{\mathbf{c}_{ki} = \left[c_{k1i}, \cdots, c_{kn_gi}\right]^T \in C^{n_g}\right\}_{i=1}^{n_g}$ be the eigenvalues and eigenvectors (with unit norm) of $\mathbf{C}_k$. It shall be shown that $\mathbf{E}_k$ has n_g eigenvalues given by $\left\{SD_k\lambda_{ki} + S_e\right\}_{i=1}^{n_g}$ with eigenvectors $\left\{\boldsymbol{\alpha}_{ki} \in C^n\right\}_{i=1}^{n_g}$, where

$$\boldsymbol{\alpha}_{ki} = \begin{bmatrix} c_{k1i}\dfrac{\mathbf{u}_1}{\left\|\mathbf{u}_1\right\|} \\ \vdots \\ c_{kn_gi}\dfrac{\mathbf{u}_{n_g}}{\left\|\mathbf{u}_{n_g}\right\|} \end{bmatrix} \qquad i = 1,..., n_g \tag{16}$$

The remaining $\left(n - n_g\right)$ eigenvalues of $\mathbf{E}_k$ are all equal to S_e with eigenvectors lying in the orthogonal complement of the subspace spanned by $\left\{\boldsymbol{\alpha}_{ki}\right\}_{i=1}^{n_g}$.

5.1 Derivation

The above results can be shown by writing $\mathcal{F}_k$ in Eq.(11) and $\mathbf{E}_k$ in Eq.(14) in a structured form:

$$\mathcal{F}_k = \begin{bmatrix} \mathbf{u}_1/\left\|\mathbf{u}_1\right\| & & \\ & \ddots & \\ & & \mathbf{u}_{n_g}/\left\|\mathbf{u}_{n_g}\right\| \end{bmatrix} \begin{bmatrix} \left\|\mathbf{u}_1\right\| & & \\ & \ddots & \\ & & \left\|\mathbf{u}_{n_g}\right\| \end{bmatrix} \begin{bmatrix} \ddot{\eta}_{k1} \\ \vdots \\ \ddot{\eta}_{kn_g} \end{bmatrix} + \boldsymbol{\varepsilon}_k \tag{17}$$
$$= \mathbf{U} diag\left\{\left\|\mathbf{u}_i\right\|\right\}_{i=1}^{n_g} \ddot{\boldsymbol{\eta}}_k + \boldsymbol{\varepsilon}_k$$

$$\mathbf{E}_k = \mathbf{U} diag\left\{\left\|\mathbf{u}_i\right\|\right\}_{i=1}^{n_g} E\left[\ddot{\boldsymbol{\eta}}_k \ddot{\boldsymbol{\eta}}_k^*\right] diag\left\{\left\|\mathbf{u}_i\right\|\right\}_{i=1}^{n_g} \mathbf{U}^T + S_e\mathbf{I}_n \tag{18}$$

where $\ddot{\boldsymbol{\eta}}_k = [\ddot{\eta}_{k1},...,\ddot{\eta}_{kn_g}]^T$ and $\mathbf{U} \in R^{n \times n_g}$ is a block-diagonal matrix formed by $\left\{\mathbf{u}_i/\left\|\mathbf{u}_i\right\|\right\}_{i=1}^{n_g}$. By noting that $E[\ddot{\boldsymbol{\eta}}_k \ddot{\boldsymbol{\eta}}_k^*]$ is a $n_g \times n_g$ matrix with (i,j) entry $SD_k\chi_{kij}$ and recalling the definition of $\mathbf{C}_k$ in Eq.(15), $\mathbf{E}_k$ in Eq.(18) can be written as:

$$\mathbf{E}_k = SD_k \mathbf{U}\mathbf{C}_k\mathbf{U}^T + S_e\mathbf{I}_n \tag{19}$$

Further substituting $\mathbf{C}_k = \sum_{i=1}^{n_g} \lambda_{ki}\mathbf{c}_{ki}\mathbf{c}_{ki}^*$ (eigenvector representation),

$$\mathbf{E}_k = \sum_{i=1}^{n_g} SD_k\lambda_{ki}\boldsymbol{\alpha}_{ki}\boldsymbol{\alpha}_{ki}^* + S_e\mathbf{I}_n \tag{20}$$

where

$$\boldsymbol{\alpha}_{ki} = \mathbf{U}\mathbf{c}_{ki} \qquad\qquad i = 1,...,n_g \tag{21}$$

Using $\mathbf{U}^T\mathbf{U} = \mathbf{I}_{n_g}$ and the orthonormal properties of $\{\mathbf{c}_{ki}\}_{i=1}^{n_g}$, i.e., $\mathbf{c}_{ki}^*\mathbf{c}_{ki} = 1$ and $\mathbf{c}_{ki}^*\mathbf{c}_{kj} = 0$ $(i \neq j)$, it can be checked that $\{\boldsymbol{\alpha}_{ki}\}_{i=1}^{n_g}$ form an orthonormal basis in a n_g-dimensional subspace. Let $\{\mathbf{a}_{ki}\}_{i=n_g+1}^{n}$ be an orthonormal basis in the orthogonal complement of this subspace. Also, let $\mathbf{a}_{ki} = \boldsymbol{\alpha}_{ki}$ ($i = 1,...,n_g$). Then $\{\mathbf{a}_{ki}\}_{i=1}^{n}$ is an orthonormal basis in C^n. Substituting $\mathbf{I}_n = \sum_{i=1}^{n} \mathbf{a}_{ki}\mathbf{a}_{ki}^*$ into Eq.(20) and collecting terms gives the eigenvector representation of $\mathbf{E}_k$:

$$\mathbf{E}_k = \sum_{i=1}^{n_g} \underbrace{\left(SD_k\lambda_{ki} + S_e\right)}_{Eigenvalue}\mathbf{a}_{ki}\mathbf{a}_{ki}^* + \sum_{i=n_g+1}^{n} \underbrace{S_e}_{Eigenvalue}\mathbf{a}_{ki}\mathbf{a}_{ki}^* \tag{22}$$

The eigenvalue properties of $\mathbf{E}_k$ claimed earlier in this section then follow.

5.2 Qualitative Analysis

The foregoing results show that for asynchronous data, the PSD matrix has n_g significant eigenvalues $\{SD_k\lambda_{ki} + S_e\}_{i=1}^{n_g}$ with eigenvectors given by Eq.(16). The remaining $(n - n_g)$ eigenvalues are all equal to S_e. This is in contrast with the case of synchronous data (see Eq.(7)), where there is only one significant eigenvalue $SD_k + S_e$ with eigenvector $\boldsymbol{\varphi}$. Because of the common dynamic amplification factor D_k in the n_g largest eigenvalues, the SV spectrum of asynchronous data looks like one with several modes with very close natural frequencies. The n_g largest eigenvalues are also proportional to $\{\lambda_{ki}\}_{i=1}^{n_g}$ (eigenvalues of $\mathbf{C}_k$ in

Eq.(15)), which depend non-trivially on the coherence χ_{kij} between different groups and the norms of the local mode shapes $\{\mathbf{u}_i\}_{i=1}^{n_g}$.

Note that $0 \le \lambda_{ki} \le 1$ $(i = 1,...,n_g)$ since the maximum eigenvalue of a matrix is less than the maximum diagonal entry. This implies that $SD_k \lambda_{ki} + S_e \le SD_k + S_e$ and so the SV spectrum of asynchronous data has smaller value (and hence apparently lower signal-to-noise ratio) than if the data were synchronous. Nevertheless, signal strength is 'conserved', in the sense that the sum of the lines in the SV spectrum (at a particular frequency) remains the same, equal to $SD_k + nS_e$ (the sum of diagonal entries of $\mathbf{E}_k$).

Consider one extreme case when all groups are synchronised, i.e., $\chi_{kij} = 1$ for all i, j. Then

$$\mathbf{C}_k = \begin{bmatrix} \|\mathbf{u}_1\| \\ \vdots \\ \|\mathbf{u}_{n_g}\| \end{bmatrix} \begin{bmatrix} \|\mathbf{u}_1\| \\ \vdots \\ \|\mathbf{u}_{n_g}\| \end{bmatrix}^T \tag{23}$$

has only one non-zero eigenvalue equal to 1, i.e., $\lambda_{k1} = 1$ and $\lambda_{ki} = 0$ $(i > 1)$. In this case $\mathbf{E}_k$ has only one significant eigenvalue equal to $SD_k + S_e$ and the remaining ones are all S_e. That is, signal strength is 'concentrated' at one single eigenvalue. This is consistent with the properties of synchronous data.

In another extreme case, consider when different groups are 'perfectly asynchronised' ($\chi_{kij} = 0$ for all $i \ne j$), and all groups have the same mode shape norm ($\|\mathbf{u}_i\| = 1/\sqrt{n_g}$ for all i). Then $\mathbf{C}_k = \mathbf{I}_n / n_g$ has all eigenvalues equal to $\lambda_{ki} = 1/n_g$ $(i = 1,...,n_g)$. In this case $\mathbf{E}_k$ has n_g identical eigenvalues equal to $SD_k / n_g + S_e$ and $(n - n_g)$ eigenvalues equal to S_e. That is, signal strength is equally spread among n_g eigenvalues. The SV spectrum exhibits n_g overlapping lines significantly above the remaining ones and varying as the dynamic amplification factor.

Finally, according to Eq.(16), the eigenvector $\boldsymbol{\alpha}_{ki}$ does not give directly the global mode shape $\boldsymbol{\varphi} = [\mathbf{u}_1;...;\mathbf{u}_{n_g}]$. The partition of $\boldsymbol{\alpha}_{ki}$ corresponding to a particular group j still gives the (normalised) local mode shape $\mathbf{u}_j / \|\mathbf{u}_j\|$ within that group. The latter, however, is scaled

in a non-trivial manner by the factor c_{kji} (related to the eigenvectors of $\mathbf{C}_k$). This has important implication on the feasibility of using the eigenvectors of PSD matrix for estimating mode shapes with asynchronous data. For example, in multiple trials of experiments, coherence is likely to vary across different data sets. The eigenvectors determined from these trials will then vary in a non-trivial and apparently random manner.

6 Identifying Mode Shape from Asynchronous Data

The discussion in Section 5.2 reveals that it is still possible to identify the natural frequencies and damping ratios from the eigenvalues of the PSD matrix of asynchronous data as they are propotional to the dynamic amplification factor. The same is not true for the mode shape, however. This section investigates the identification of mode shape from asynchronous data. A simple empirical method is proposed for this purpose.

In the eigenvector of the PSD matrix with significant eigenvalue, different partitions $\mathbf{u}_i$ of the global mode shape $\boldsymbol{\varphi}$ are scaled in a non-trivial manner depending on the coherence among groups. The normalised local mode shape $\bar{\mathbf{u}}_i = \mathbf{u}_i / \|\mathbf{u}_i\|$ in each group can be determined easily by either analysing the data of the group in isolation or by normalising the corresponding partition of the eigenvector of the PSD matrix. The main problem therefore lies in the determination of the scaling factors $\{\|\mathbf{u}_i\|\}_{i=1}^{n_g}$ to give the correct mode shape $\boldsymbol{\varphi} = [\|\mathbf{u}_1\|\bar{\mathbf{u}}_1; ...; \|\mathbf{u}_{n_g}\|\bar{\mathbf{u}}_{n_g}]$. Although the eigenvalue properties of $\mathbf{C}_k$ have been obtained analytically in terms of $\{\|\mathbf{u}_i\|\}_{i=1}^{n_g}$, determing the latter from the former is difficult as it involves an inverse problem, not to mention the need to estimate the coherence factors.

The method proposed here makes use of the fact that the data in different groups, regardless of their degree of synchronisation, are measured within the same time span and hence subjected to the same ambient excitation. When the data of different groups are analysed separately, their identified value of modal force PSD are related to the scaling of the mode shape. By enforcing a common scaling in modal force PSD among different groups, the scaling factor $\{\|\mathbf{u}_i\|\}_{i=1}^{n_g}$ of mode shapes can be determined.

Specifically, suppose one analyses in isolation the data in the ith group to obtain an estimate for the normalised local mode shape $\bar{\mathbf{u}}_i$ (with $\|\bar{\mathbf{u}}_i\| = 1$) and modal force PSD S_i'. These can

be obtained empirically from the eigenvalue properties of the PSD matrix within the group. In a more sophisticated manner, they can be identified by fast Bayesian method in the frequency domain [39]. The values of S_i' differ for different groups because their mode shapes do not have the same scaling. Note that the modal contribution to physical response, $\mathbf{u}_i\ddot{\eta}(t)$, is invariant to scaling. Also, the PSD of $\ddot{\eta}$ is proportional to the modal force PSD. These imply that if the mode shape is scaled by a factor, the modal response $\ddot{\eta}$ must be scaled down by the same factor, and the modal force PSD by the square of that factor. In the global mode shape $\boldsymbol{\varphi} = [\|\mathbf{u}_1\|\overline{\mathbf{u}}_1;...;\|\mathbf{u}_{n_g}\|\overline{\mathbf{u}}_{n_g}]$, the partition corresponding to the ith group is $\|\mathbf{u}_i\|\overline{\mathbf{u}}_i$ but the one when the ith group data is analysed in isolation is $\overline{\mathbf{u}}_i$. That is, compared to the former, the latter is scaled down by $\|\mathbf{u}_i\|$. This means that if S is the modal force PSD consistent with the scaling of $\boldsymbol{\varphi}$ ($\|\boldsymbol{\varphi}\| = 1$), then $S_i' = S\|\mathbf{u}_i\|^2$ is the counterpart consistent with $\overline{\mathbf{u}}_i$ ($\|\mathbf{u}_i\| = 1$). Note that S does not depend on i because all groups are measured under the same excitation. This relationship implies that $\|\mathbf{u}_i\| \propto \sqrt{S_i'}$. Further requiring $\|\boldsymbol{\varphi}\|^2 = \sum_{i=1}^{n_g}\|\mathbf{u}_i\|^2 = 1$ leads to the estimation formula

$$\|\mathbf{u}_i\| = \sqrt{\frac{S_i'}{\sum_{j=1}^{n_g} S_j'}} \tag{24}$$

As the local mode shapes are obtained in isolation, the relative direction between them should be further determined in order to obtain the correct global mode shape. This can be done based on physical intuition, e.g., spatial continuity of mode shapes.

7 Verification Examples

In this section, the theoretical eigenvalue properties of the PSD matrix derived in Section 5 will be validated. The first example is based on synthetic data generated using an imperfect coherence model, where there is no modelling error. The second example is based on real laboratory data where the validity of the coherence model proposed in Section 4 will also be investigated.

7.1 Simulated Data

Consider a set of synthetic data generated for 1000s at 100Hz according to

$$\ddot{\mathbf{x}}(t)=\begin{bmatrix}\mathbf{u}_1\ddot{\eta}_1(t)\\ \mathbf{u}_2\ddot{\eta}_2(t)\end{bmatrix}+\boldsymbol{\varepsilon}(t) \tag{25}$$

where $\mathbf{u}_1=[1 \quad 2 \quad 3]^T/\sqrt{91}$ and $\mathbf{u}_2=[4 \quad 5 \quad 6]^T/\sqrt{91}$ (check that $\|\mathbf{u}_1\|^2+\|\mathbf{u}_2\|^2=1$); $\ddot{\eta}_1$ and $\ddot{\eta}_2$ are modal acceleration response satisfying $\ddot{\eta}_i(t)+2\zeta\omega\dot{\eta}_i(t)+\omega^2\eta_i(t)=p_i(t)$; $\omega=2\pi$ rad/s (i.e. $f=1$Hz) and $\zeta=1\%$; p_1 and p_2 are white noise modal forces with PSD $S=1\times10^{-8}\,\mathrm{g}^2/\mathrm{Hz}$; $\boldsymbol{\varepsilon}(t)\in R^{6\times1}$ is white noise measurement error with PSD $S_e=1\times10^{-7}\,\mathrm{g}^2/\mathrm{Hz}$. The modal signal-to-noise ratio in terms of PSD at natural frequency is about $S/(4\zeta^2S_e)\approx250$, typical for good quality OMA data. The modal forces are generally correlated, with a coherence of χ . Clearly, there are six measured DOFs. The first three DOFs are synchronised, and so are the last three. There are thus two synchronous data groups, comprising the first three and last three DOFs, respectively. Note that the coherence of modal response between these two groups is equal to the coherence between their modal forces. The eigenvalue properties of the PSD matrix shall be verified for different values of χ .

Consider six scenarios with increasing coherence, i.e., $\chi=0$ (perfectly asynchronous), 0.2, 0.4, 0.6, 0.8, 1 (synchronous). For each scenario, the sample PSD matrix of data is obtained according to Eq.(10) by averaging those from $M=40$ non-overlapping segments (each 25s), which gives a frequency resolution of 1/25=0.04Hz. Figure 4 shows the root SV spectrum for these six scenarios. The solid line shows the square root of eigenvalues of the sample PSD. The dashed line shows the theoretical value calculated according to Eq.(22) using the given values of coherence and modal properties. These two lines almost coincide, verifying the correctness of the theoretical prediction. Although omitted here, the eigenvectors predicted by Eq.(16) have also been verified to agree with those of the sample PSD matrix at the natural frequency, with a MAC (Modal Assurance Criteria) of almost 1 (to 4 decimal places).

7.2 Laboratory Data

The next example serves to verify that the theoretical characteristics of the SV spectrum derived based on imperfect coherence (which is empirical) can also provide a good prediction for real asynchronous data. Consider again the laboratory data in Section 3, where Sensor A is synchronised with B but not with C. According to Eq.(22), the theoretical eigenvalues of the PSD matrix depend on the modal properties and the coherence between modal responses of different groups. These shall be estimated first from measured data.

According to Eq.(13), the coherence χ_{kij} between the ith and jth sensor group refers to the coherence between the modal responses $\ddot{\eta}_{ki}$ and $\ddot{\eta}_{kj}$. However, only the FFT $\{\mathcal{F}_k\}$ of the data can be obtained (see Eq.(3)), which includes the modal responses as well as measurement noise (see Eq.(11)). In view of this, χ_{kij} is estimated using the FFT near the resonance peak where modal response dominates. Figure 5 shows the real part of the coherence for the synchronous data set (Sensor A & B) and asynchronous data set (Sensor A & C). The real part is shown as it can also detect constant time shift in general situations. The coherence for synchronous data set is very close to 1 around the resonance peak of the mode. For asynchronous data set, the coherence is lower than 1.

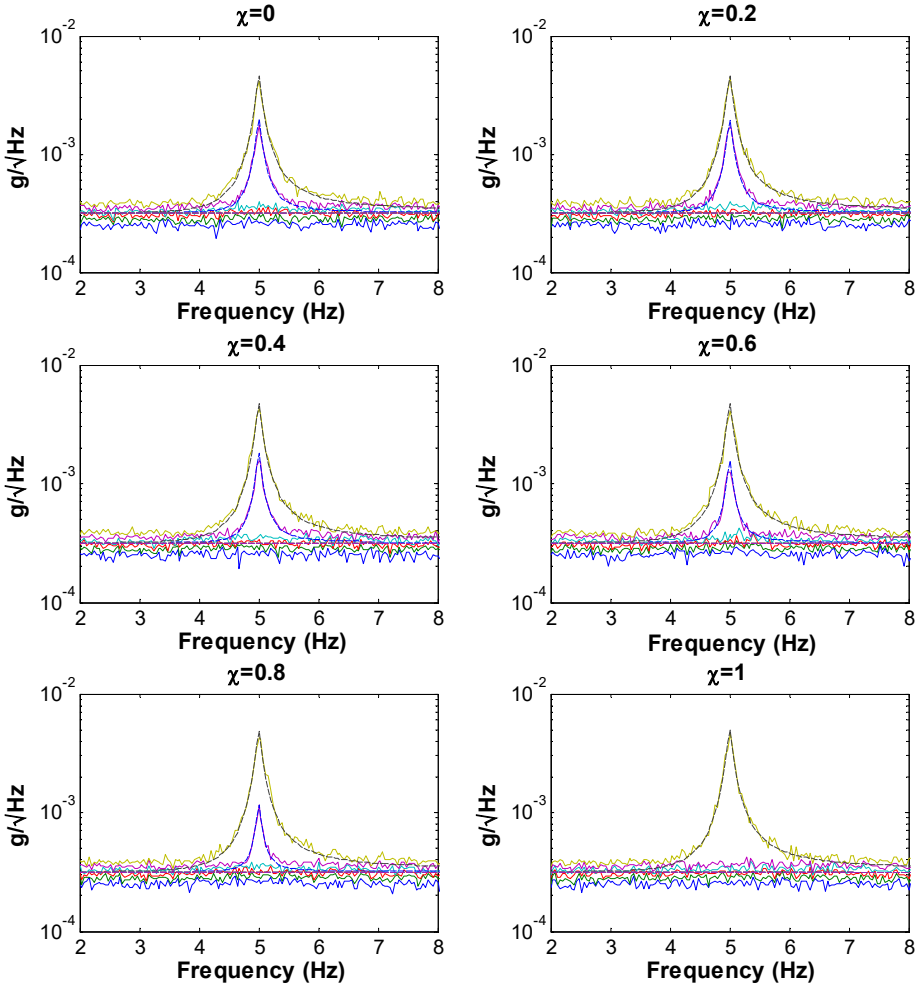

Figure 4. Root SV Spectrum Estimated from Sample PSD (Solid line) and Theoretical Values (Eq.(22), Dashed line) for Different Values of Coherence χ

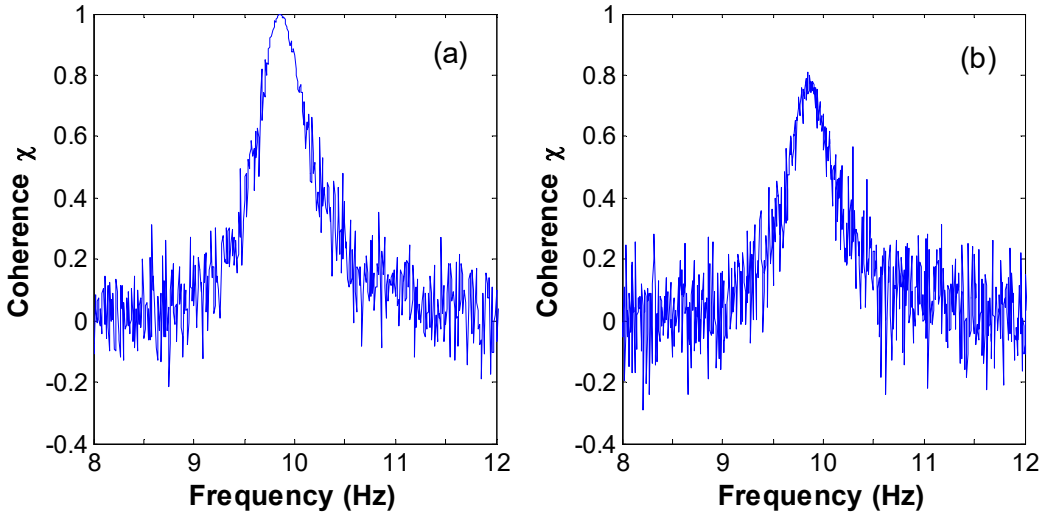

Figure 5. Real Part of Coherence for (a) Synchronous Data Set (Sensor A & B) (b) Asynchronous Data Set (Sensor A & C)

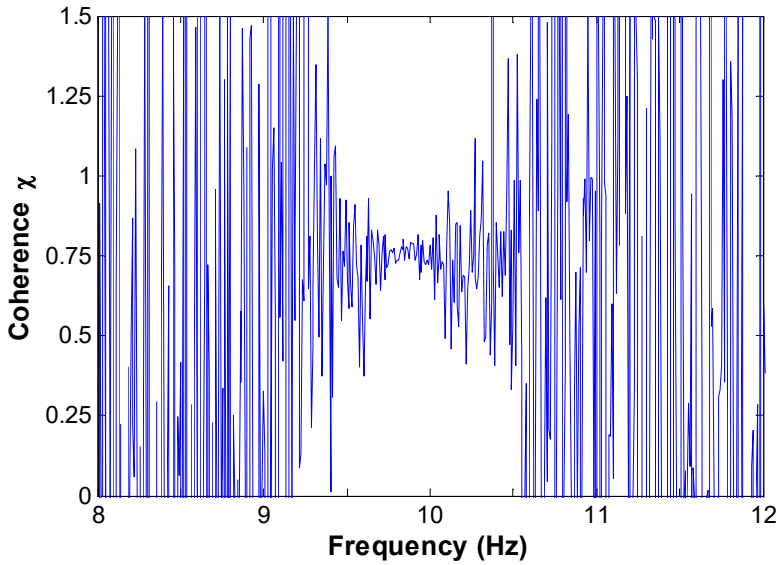

Figure 6. Coherence Estimated as Ratio of Figure 5(b) to Figure 5(a)

Note that even for the synchronous data set, coherence drops for frequencies away from the resonance peak because there the FFT is no longer dominated by modal response. The ratio of the coherence of the asynchronous data set (Figure 5(b)) to the synchronous data set (Figure 5(a)) is plotted in Figure 6. The ratio does not vary significantly within the resonance band. Assuming that the coherence of synchronous data set near the natural frequency is one,

the coherence near the resonance peak for the asynchronous data set can be assumed to be constant, which is estimated by averaging to be 0.79.

Next, modal properties are estimated from the synchronous data set using Bayesian FFT method [39]. Using the FFT in the band $[9.6 \quad 10.1]$Hz (hand-picked) yields a most probable value of $f = 9.855$Hz (natural frequency), $\zeta = 0.17\%$ (damping ratio), $\sqrt{S} = 2.35\mu g/\sqrt{\text{Hz}}$ (root modal force PSD) and $\sqrt{S_e} = 27.1\mu g/\sqrt{\text{Hz}}$ (root measurement noise PSD). The identified mode shape is $[0.71 \quad 0.71]^T$, which is consistent with the fact that Sensor A and B measure the same DOF. These estimates are determined to be sufficiently accurate. For example, the posterior c.o.v. (coefficient of variation = standard deviation / most probable value) of damping ratio is only 4%.

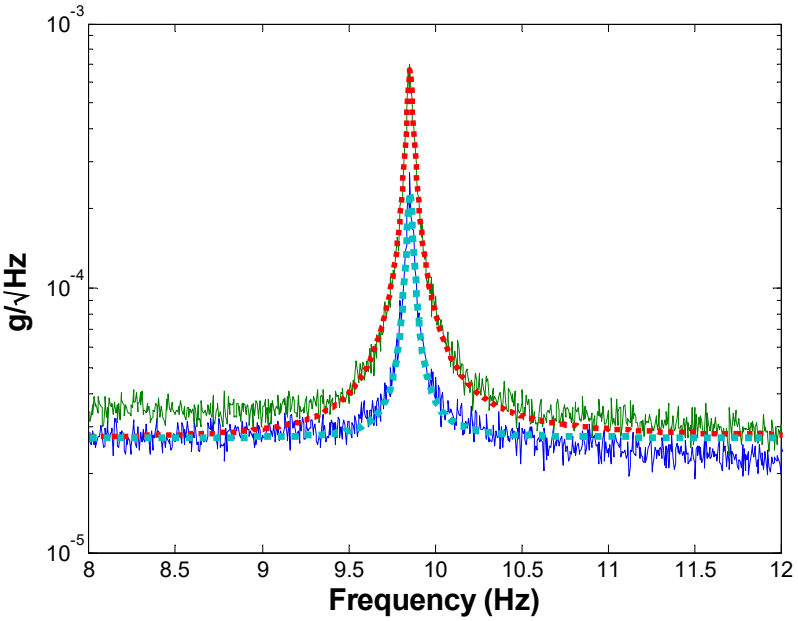

Figure 7. Root SV Spectrum of Asynchronous Data Set (Sensor A & C) from Eigenvalues of Sample PSD (Solid line) and Theoretical Values (Dashed line)

Using the identified values of modal parameters and coherence, the theoretical eigenvalues of the PSD matrix for asynchronous data set are calculated using Eq.(22). The results are shown in Figure 7. The theoretical prediction agrees with the values directly calculated from the sample PSD, demonstrating its applicability with real asynchronous data. Multiple trials of data have been investigated (results omitted here), showing qualitatively similar agreement.

8 Application Example

In this section an example is presented to investigate modal identification with real asynchronous data. Modal properties are identified from existing algorithm that assumes synchronous data and associated issues are explored. Mode shapes are also identified using the method proposed in Section 6.

The instrumented structure is a four-storey aluminium frame, measuring 30cm×20cm in plan with a uniform storey height of 25cm, as shown in Figure 8(a). Piezoelectric accelerometers and DAQ hardware used in this example are the same as those in Section 3. Accelerometers are distributed at the centre of each floor. The acceleration response of each floor in the weak direction (parallel to paper) under ambient condition (i.e., random natural excitation such as microtremor and cultural activities) is measured. Figure 8(b) shows a schematic setup of the sensors. Sensor 1 to 4 are synchronised using one DAQ hardware and sensor 5 & 6 are synchronised using another. All data channels are controlled to start recording data at the same time with the same sampling rate of 2048Hz for 30 minutes. The data is later decimated to 256Hz for analysis. The data comprising channels 1 to 4 is referred as the synchronous data set. The data comprising channels {1,2,5,6} is referred as the asynchronous data set, where there are two synchronous groups, {1,2} and {5,6}.

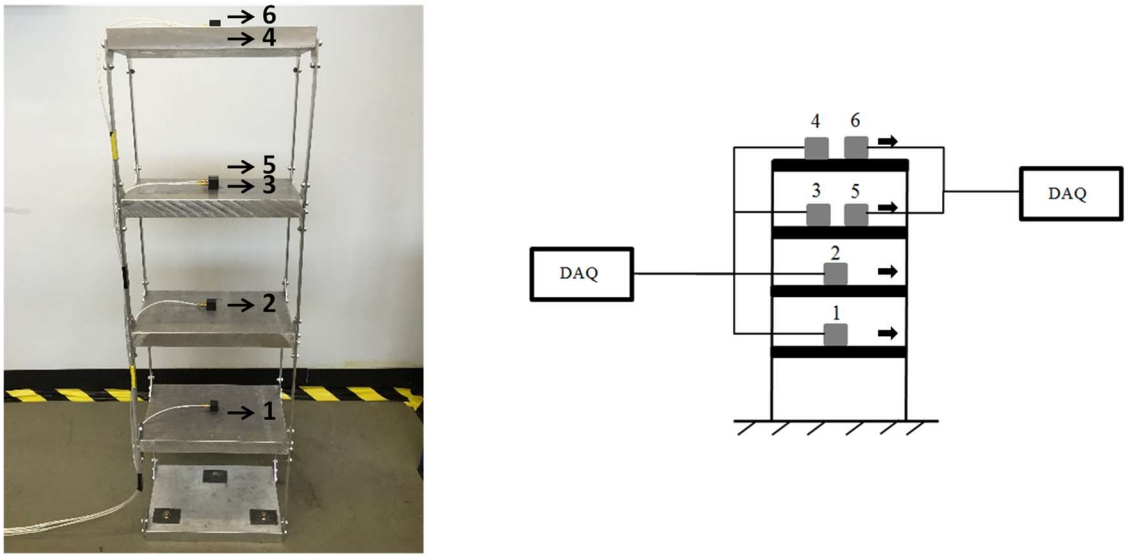

(a) (b)

Figure 8. Four-storey Lab Frame (a) Laboratory Photo (b) Schematic Setup

The root SV spectrum for synchronous and asynchronous data sets are plotted in Figure 9 and Figure 10, respectively. For synchronous data, the number of significant peaks in a resonance band indicates the number of modes in the band. Figure 9 indicates five well-separated modes,

each evidenced by a single (top) line taking the shape of dynamic amplification factor. In Figure 10, there are two lines significantly above the remaining ones for each mode, consistent with the fact that there are two asynchronous groups of data channels.

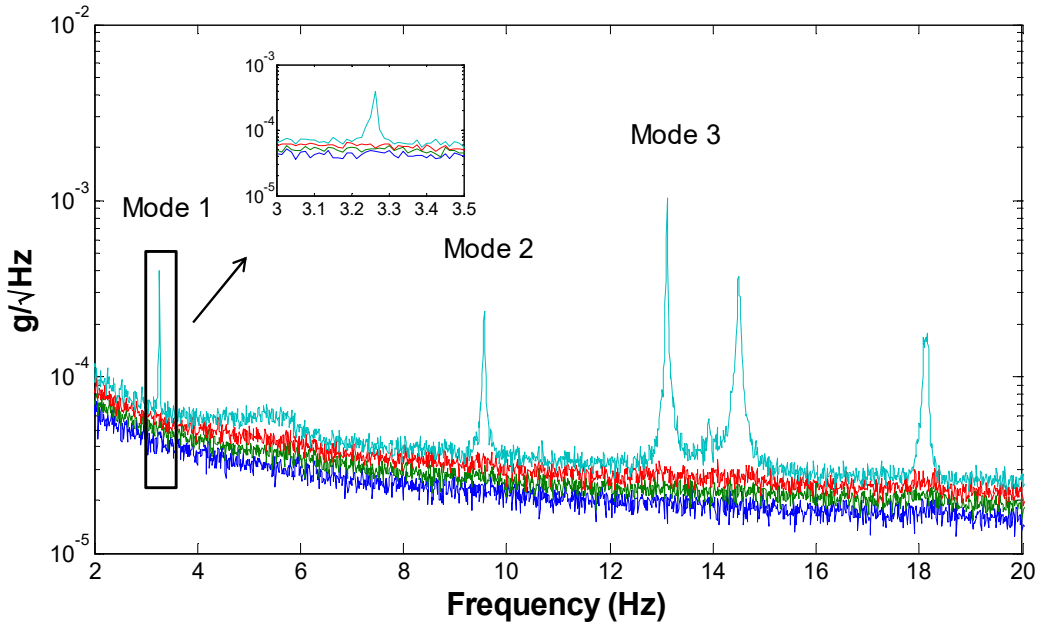

Figure 9. Root SV Spectrum of Synchronous Data Set

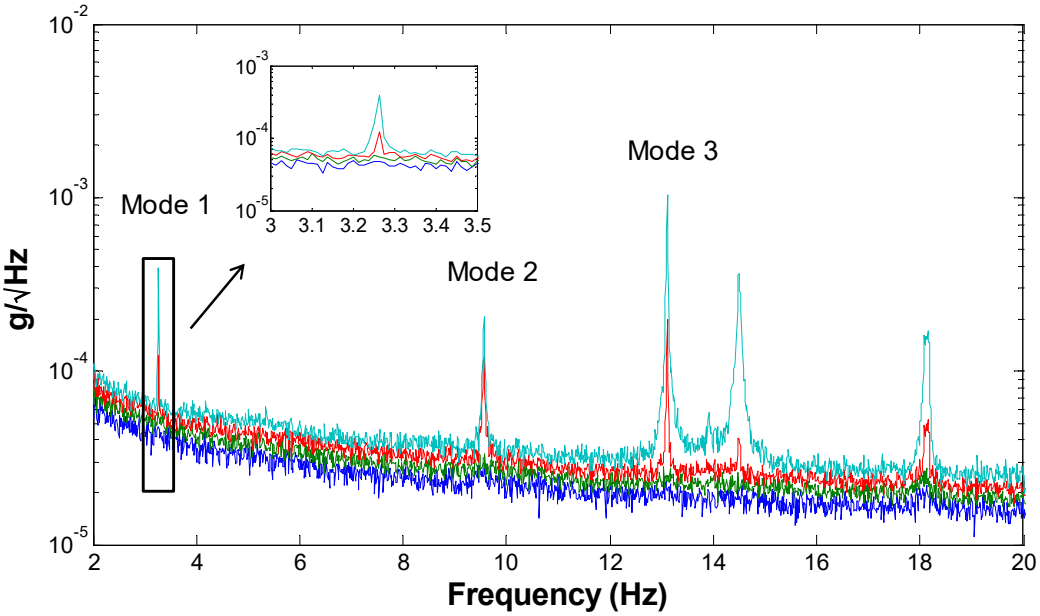

Figure 10. Root SV Spectrum of Asynchronous Data Set

8.1 Identifying Modal Properties (Except Mode Shape)

The modal properties of three modes marked in Figure 10 are identified based on synchronous and asynchronous data sets using fast Bayesian FFT method [39]. Although the algorithm was originally developed for synchronous data, it is applied here to investigate potential issues when applied to asynchronous data. The frequency bands selected (hand-picked) to identify Mode 1 to 3 are $[3.25 \quad 3.27]$Hz, $[9.50 \quad 9.60]$Hz and $[13.06 \quad 13.16]$Hz, respectively. The identification results, including the most probable values (MPV) and posterior c.o.v. are listed in Table 1. The natural frequencies and damping ratios identified based on the asynchronous data set are close to their counterparts based on the synchronous data set. This is also true for the modal force PSDs. However, the prediction error PSDs identified based on the asynchronous set are larger than the ones for the synchronous data set. This is a reflection of modelling error due to asynchronous data.

Table 1. Identified Modal Parameters, Four-storey Lab Frame

Parameter	Mode	Synchronous Data Set		Asynchronous Data Set	
		MPV	c.o.v. (%)	MPV	c.o.v. (%)
$f\,(\mathrm{Hz})$	1	3.260	0.01	3.260	0.02
	2	9.559	0.02	9.560	0.02
	3	13.10	0.06	13.10	0.06
$\zeta\,(\%)$	1	0.07	29.3	0.07	30.3
	2	0.15	13.4	0.11	16.0
	3	0.04	15.4	0.04	15.8
$\sqrt{S}\,(\mu g/\sqrt{\mathrm{Hz}})$	1	0.89	12.7	0.89	14.0
	2	0.76	6.65	0.50	8.20
	3	1.03	4.47	1.00	4.71
$\sqrt{S_e}\,(\mu g/\sqrt{\mathrm{Hz}})$	1	54.1	4.74	78.2	4.74
	2	28.1	2.11	54.4	2.12
	3	25.1	2.15	58.6	2.14

8.2 Identifying Mode Shape using Conventional Method

The results so far suggest that the natural frequency and damping ratio are not severely affected even when they are identified from asynchronous data using an algorithm assuming synchronous data. The major issue of asynchronisation in modal identification lies in the identified mode shapes. Figure 11 shows the identified mode shapes (MPV) from the synchronous (solid line) and asynchronous data sets (dashed line with circles). The MAC values between the mode shapes of these two sets for Mode 1 to 3 are 0.997, 0.393 and 0.637, respectively. Recall that for the asynchronous data set, channels {1,2} (measuring floor 1 & 2) are not synchronised with {5,6} (measuring floor 3 & 4). The relative scaling between the partial mode shapes of these two groups are not the same as the one for the synchronous data set. For Mode 2 and 3, the relative direction also changes. This is typical when using asynchronous data for identifying mode shape.

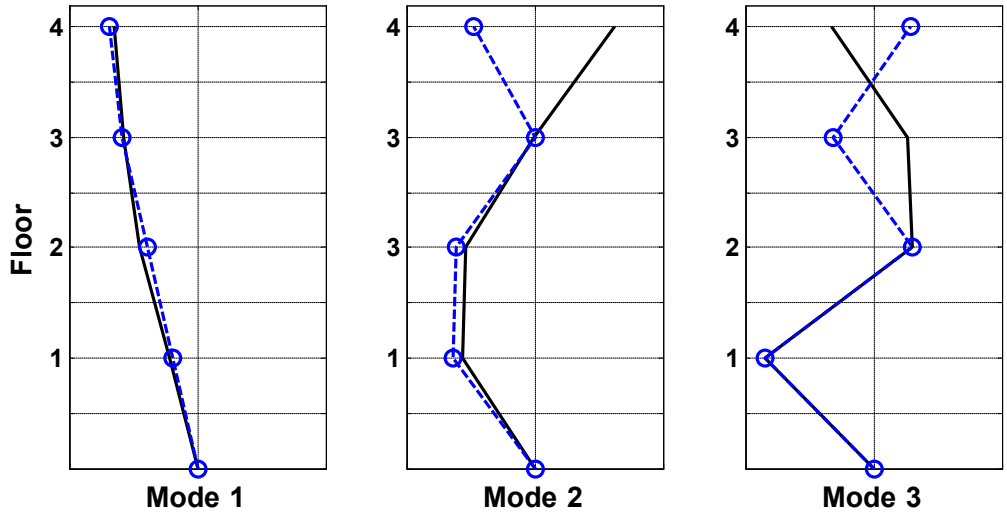

Figure 11. Identified Mode Shapes (MPV); Solid Line-Synchronous Data Set, Dashed Line with Circles-Asynchronous Data Set

8.3 Identifying Mode Shape using Proposed Method

To obtain the correct mode shape from the asynchronous data set, the method proposed in Section 6 is used. Here, the global mode shape is $\boldsymbol{\varphi} = [\|\mathbf{u}_1\|\bar{\mathbf{u}}_1; \|\mathbf{u}_2\|\bar{\mathbf{u}}_2]$, where $\bar{\mathbf{u}}_1$ and $\bar{\mathbf{u}}_2$ (normalised to unit norm) are the local mode shapes of floor {1,2} and {3,4}, respectively; the scaling factors $\|\mathbf{u}_1\|$ and $\|\mathbf{u}_2\|$ are estimated based on Eq.(24), i.e., $\|\mathbf{u}_i\| = \sqrt{S_i'/(S_1' + S_2')}$ ($i = 1,2$) where S_i' is the modal force PSD consistent with scaling of mode shape $\bar{\mathbf{u}}_i$. Note

that $\overline{\mathbf{u}}_1$ and S_1' are identified using the data of floor {1,2} only, $\overline{\mathbf{u}}_2$ and S_2' use the data of floor {3,4} only.

Table 2 shows the identified values of S_i'. Based on the MPVs, the scaling factors and hence the global mode shape can be determined, which is shown in Figure 12 as dashed line with squares. It almost coincides with the mode shape identified using synchronous data (solid line). The MAC values are calculated to be 0.9989, 0.9996 and 0.9975 for Mode 1 to 3 respectively. This demonstrates that the proposed method can determine correctly the global mode shape from asynchronous data.

Table 2. Identified Modal Force PSD

Mode	S_1' [(μg)^2/Hz] Channel 1 & 2		S_2' [(μg)^2/Hz] Channel 5 & 6	
	MPV	c.o.v. (%)	MPV	c.o.v. (%)
1	0.2018	31	0.7613	27
2	0.3234	13	0.2242	15
3	0.8778	9	0.2243	9

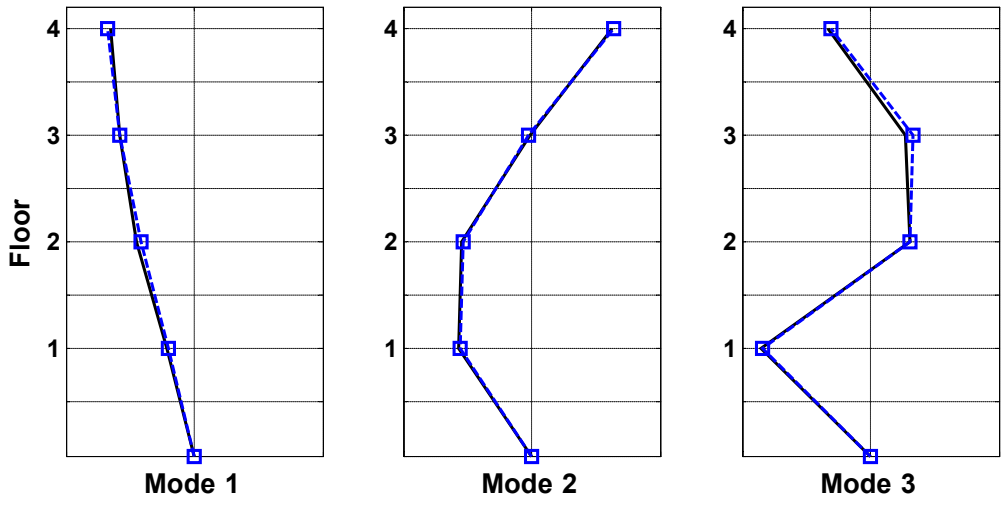

Figure 12. Identified Mode Shape (MPV); Solid Line-Synchronous Data Set, Dashed Line with Squares-Asynchronous Data Set using Proposed Method

9 Conclusions

This paper has investigated the problem of imperfect synchronisation in operational modal analysis (OMA). It addresses the fact that, even when data of multiple channels can start from the same time (by hardware or correction after acquisition), when measured by asynchronous clocks they are subjected to random time drifts that are difficult to correct (if possible) after digital sampling. This is the primary issue if one wants to perform OMA with asynchronous data. Asynchronous data is generally a non-stationary stochastic process, which is difficult to model or analyse. A stationary stochastic model has been proposed, which is conducive to analysis while retaining the characteristics of asynchronous data over suitable time scales. The theoretical PSD matrix near the natural frequency of a single mode has been derived. Its eigenvalues and eigenvectors have been obtained analytically in terms of modal properties and coherence parameters capturing asynchronous characteristics. In contrast with the case of synchronous data where there is only one significant eigenvalue, for asynchronous data there are as many significant eigenvalues as the number of synchronous data groups. The corresponding eigenvectors do not give directly the global mode shape but depend non-trivially on the coherence parameters as well as the norms of the local mode shapes of different synchronous data groups. The proposed stochastic model for asynchronous data and the theoretical properties of its PSD matrix have been verified using synthetic and experimental data.

Although conventional methods do not allow the global mode shape to be determined from asynchronous data, the present work reveals the possibility by noting the simple but crucial fact that the data from different groups are measured under the same time span and ambient excitation, and hence share a common PSD in the modal force. Making use of this fact, a simple method has been proposed for determining the global mode shape from asynchronous data. For perfectly incoherent data groups, it is not possible to determine the relative sense ($\pm$) of their local mode shapes, which is a fundamental limitation of such data. In implementation, the sense can be determined from intuition (feasible for low frequency modes) or estimated from the residual coherence between data groups.

The proposed method has been applied to identifying the mode shapes of a laboratory structure, which reveals the modal identification precision and issues encountered in OMA with asynchronous data. The identified natural frequencies and damping ratios are not severely affected even when asynchronous data is (inappropriately) processed by

conventional modal identification method assuming synchronous data. The major problem lies in the mode shapes, where the relative scaling and direction between the local mode shapes of different data groups is erroneously determined. As demonstrated by the example, the global mode shape can be correctly determined using the proposed method that makes use of the identified values of modal force PSD.

It is hoped that this work provides the pathway for even more flexible and economical implementation of ambient vibration tests and OMA. For example, one future possibility is to use smart phones for quick OMA, whose data need not be synchronised.

Acknowledgments

This paper was partly supported by Tung Doctoral Scholarship and UK Engineering & Physical Sciences Research Council (EP/N017897/1). The financial support is gratefully acknowledged.

References

1. Hudson DE. Dynamic Tests of Full-Scale Structures. *Journal of the Engineering Mechanics Division* 1977; **103**(6): 1141–1157.

2. Ewins DJ. *Modal testing : theory, practice, and application*. Baldock : Research Studies Press, 2000.; 2000.

3. Farrar CR, Worden K. An introduction to structural health monitoring. *Philosophical Transactions Series A, Mathematical, Physical, and Engineering Sciences* 2007; **365**(December 2006): 303–315. DOI: 10.1098/rsta.2006.1928.

4. Hearn G, Testa R. Modal analysis for damage detection in structures. *Journal of Structural Engineering* 1991; **117**(10): 3042–3063.

5. Rahai A, Bakhtiari-Nejad F, Esfandiari A. Damage Assessment of Structure using Incomplete Measured Mode Shapes. *Structural Control and Health Monitoring* 2006; **14**(5): 808–829. DOI: 10.1002/stc.183.

6. Ivanovic SS, Trifunac MD, Todorovska MI. Ambient Vibration Tests of Structure-A Review. *Journal of Earthquake Tecknology* 2000; **37**(4): 165–197.

7. Brownjohn JMW. Ambient vibration studies for system identification of tall buildings.

Earthquake Engineering and Structural Dynamics 2003; **32**(April 2002): 71–95. DOI: 10.1002/eqe.215.

8. Wenzel H, Pichler D. *Ambient vibration monitoring*. Wiley, UK; 2005.

9. Brincker R, Zhang L, Andersen P. Modal identification of output-only systems using frequency domain decomposition. *Smart Materials and Structures* 2001; **10**(3): 441–445. DOI: 10.1088/0964-1726/10/3/303.

10. Peeters B, De Roeck G. Stochastic System Identification for Operational Modal Analysis: A Review. *Journal of Dynamic Systems, Measurement, and Control* 2001; **123**(4): 659. DOI: 10.1115/1.1410370.

11. Antoni J. Blind separation of vibration components: Principles and demonstrations. *Mechanical Systems and Signal Processing* 2005; **19**(6): 1166–1180. DOI: 10.1016/j.ymssp.2005.08.008.

12. Poncelet F, Kerschen G, Golinval JC, Verhelst D. Output-only modal analysis using blind source separation techniques. *Mechanical Systems and Signal Processing* 2007; **21**(6): 2335–2358. DOI: 10.1016/j.ymssp.2006.12.005.

13. Sadhu A, Narasimhan S. A decentralized blind source separation algorithm for ambient modal identification in the presence of narrowband disturbances. *Structural Control and Health Monitoring* 2014; **21**(3): 282–302.

14. Guillaume P, Verboven P, Vanlanduit S. Frequency-domain maximum likelihood identification of modal parameters with confidence intervals. *Proceedings of the International Seminar on Modal Analysis*, vol. 1, 1998.

15. Parloo E, Guillaume P, Cauberghe B. Maximum likelihood identification of non-stationary operational data. *Journal of Sound and Vibration* 2003; **268**(5): 971–991. DOI: 10.1016/S0022-460X(03)00377-8.

16. Oh BK, Hwang JW, Kim Y, Cho T, Park HS. Vision-based system identification technique for building structures using a motion capture system. *Journal of Sound and Vibration* 2015; **356**: 72–85. DOI: 10.1016/j.jsv.2015.07.011.

17. Au SK, Zhang FL, Ni YC. Bayesian operational modal analysis: Theory, computation, practice. *Computers & Structures* 2013; **126**: 3–14. DOI: 10.1016/j.compstruc.2012.12.015.

18. Mills DL. Internet time synchronization: the network time protocol. *IEEE Transactions on Communications* 1991; **39**(10): 1482–1493. DOI: 10.1109/26.103043.

19. Kaplan E, Hegarty C. *Understanding GPS: principles and applications*. Artech house; 2005.

20. Lynch JP. A Summary Review of Wireless Sensors and Sensor Networks for Structural Health Monitoring. *The Shock and Vibration Digest* 2006; **38**(2): 91–128. DOI: 10.1177/0583102406061499.

21. Linderman LE, Mechitov KA, Spencer BF. TinyOS-based real-time wireless data acquisition framework for structural health monitoring and control. *Structural Control and Health Monitoring* 2013; **20**(6): 1007–1020. DOI: 10.1002/stc.1514.

22. Chen Z, Casciati F. A low-noise, real-time, wireless data acquisition system for structural monitoring applications. *Structural Control and Health Monitoring* 2014; **21**(7): 1118–1136. DOI: 10.1002/stc.1636.

23. Elson J, Girod L, Estrin D. Fine-grained network time synchronization using reference broadcasts. *ACM SIGOPS Operating Systems Review* 2002; **36**(SI): 147–163. DOI: 10.1145/844128.844143.

24. Ganeriwal S, Kumar R, Srivastava MB. Timing-Sync Protocol for Sensor Networks. *Proceedings of the 1st ACM International Conference on Embedded Networked Sensor Systems*, 2003. DOI: 10.1145/958507.958508.

25. Ye Q, Zhang Y, Cheng L. A study on the optimal time synchronization accuracy in wireless sensor networks. *Computer Networks* 2005; **48**(4): 549–566. DOI: 10.1016/j.comnet.2004.10.018.

26. Krishnamurthy V, Fowler K, Sazonov E. The effect of time synchronization of wireless sensors on the modal analysis of structures. *Smart Materials and Structures* 2008; **17**: 55018. DOI: 10.1088/0964-1726/17/5/055018.

27. Lynch JP, Wang Y, Law KH, Yi JH, Lee CG, Yun CB. Validation of a large-scale wireless structural monitoring system on the Geumdang Bridge. *Proceedings of the 9th International Conference on Structural Safety and Reliability*, 2005.

28. Yan G, Dyke SJ. Structural damage detection robust against time synchronization errors. *Smart Materials and Structures* 2010; **19**(6): 65001. DOI: 10.1088/0964-

1726/19/6/065001.

29. Park JH, Kim JT, Na WB, Woo J. Output-only Modal Analysis Approach for Time-Unsynchronization Signals in Wireless Sensor Network. *Proceedings of SPIE - The International Society for Optical Engineering*, vol. 7295, 2009. DOI: 10.1117/12.816264.

30. Gerber EA, Ballato A. *Precision frequency control*. vol. 1. 1985.

31. Vig JR. Introduction to Quartz Frequency Standards 1992.

32. Brillinger DR. *Time series: data analysis and theory*. vol. 36. Siam; 1981.

33. Au SK. Fast Bayesian ambient modal identification in the frequency domain, Part I: Posterior most probable value. *Mechanical Systems and Signal Processing* 2012; **26**: 60–75. DOI: 10.1016/j.ymssp.2011.06.017.

34. Welch P. The use of fast Fourier transform for the estimation of power spectra: A method based on time averaging over short, modified periodograms. *Audio and Electroacoustics, IEEE Transactions on* 1967; **15**(2): 70–73.

35. Demir A, Mehrotra A, Roychowdhury J. Phase noise in oscillators: A unifying theory and numerical methods for characterization. *Circuits and Systems I: Fundamental Theory and Applications, IEEE Transactions on* 2000; **47**(5): 655–674. DOI: 10.1109/81.847872.

36. Löhning M, Fettweis G. The effects of aperture jitter and clock jitter in wideband ADCs. *Computer Standards and Interfaces* 2007; **29**(1): 11–18. DOI: 10.1016/j.csi.2005.12.005.

37. Bjorklund S, Ljung L. A review of time-delay estimation techniques. *42nd IEEE International Conference on Decision and Control (IEEE Cat. No.03CH37475)*, vol. 3, 2003. DOI: 10.1109/CDC.2003.1272997.

38. Jacovitti G, Scarano G. Discrete time techniques for time delay estimation. *IEEE Transactions on Signal Processing* 1993; **41**(2): 525–533. DOI: 10.1109/78.193195.

39. Au SK. Fast Bayesian FFT method for ambient modal identification with separated modes. *Journal of Engineering Mechanics* 2011. DOI: 10.1061/(ASCE)EM.1943-7889.0000213.